



A Musculoskeletal Model Driven by Dual Microsoft Kinect Sensor Data

Skals, Sebastian; Rasmussen, Kasper Phil; Bendtsen, Kaare Moss; Yang, Jian; Andersen, Michael Skipper

Published in:
Multibody System Dynamics

DOI (link to publication from Publisher):
[10.1007/s11044-017-9573-8](https://doi.org/10.1007/s11044-017-9573-8)

Publication date:
2017

Document Version
Accepted author manuscript, peer reviewed version

[Link to publication from Aalborg University](#)

Citation for published version (APA):
Skals, S., Rasmussen, K. P., Bendtsen, K. M., Yang, J., & Andersen, M. S. (2017). A Musculoskeletal Model Driven by Dual Microsoft Kinect Sensor Data. *Multibody System Dynamics*, 41(4), 297-316.
<https://doi.org/10.1007/s11044-017-9573-8>

General rights

Copyright and moral rights for the publications made accessible in the public portal are retained by the authors and/or other copyright owners and it is a condition of accessing publications that users recognise and abide by the legal requirements associated with these rights.

- Users may download and print one copy of any publication from the public portal for the purpose of private study or research.
- You may not further distribute the material or use it for any profit-making activity or commercial gain
- You may freely distribute the URL identifying the publication in the public portal -

Take down policy

If you believe that this document breaches copyright please contact us at vbn@aub.aau.dk providing details, and we will remove access to the work immediately and investigate your claim.

A Musculoskeletal Model Driven by Dual Microsoft Kinect Sensor Data

Sebastian Skals¹, Kasper P. Rasmussen², Kaare M. Bendtsen³, Jian Yang⁴,

Michael S. Andersen⁴

¹National Research Centre for the Working Environment, Lersø Parkallé 105, DK-2100 Copenhagen East, Denmark

²AnyBody Technology A/S, Niels Jernes Vej 10, DK-9220 Aalborg East, Denmark

³Department of Health Science and Technology, Aalborg University, Fredrik Bajers Vej 7D, DK-9220 Aalborg East, Denmark

⁴Department of Mechanical and Manufacturing Engineering, Aalborg University, Fibigerstraede 16, DK-9220 Aalborg East, Denmark

Corresponding author:

Michael Skipper Andersen, M.Sc.E.E., Ph.D.

Phone: +45-99409311

Mobile: +45-30354170

E-mail: msa@m-tech.aau.dk

Acknowledgements:

This work was supported by the Danish Agency for Science, Technology and Innovation under the Patient@Home project to M. S. Andersen and J. Yang and the Danish Council for Independent Research under grant number DFF-4184-00018 to M. S. Andersen.

Abstract

Musculoskeletal modelling is becoming a standard method to estimate muscle, ligament and joint forces non-invasively. As input, these models often use kinematic data obtained using marker-based motion capture, which, however, is associated with several limitations, such as soft tissue artefacts and the time-consuming task of attaching markers. These issues can potentially be addressed by applying marker-less motion capture. Therefore, we developed a musculoskeletal model driven by marker-less motion capture data, based on two Microsoft Kinect Sensors and iPi Motion Capture software, which incorporated a method for predicting ground reaction forces and moments. For validation, selected model outputs (e.g. ground reaction forces, joint reaction forces, joint angles and joint range-of-motion) were compared to musculoskeletal models driven by simultaneously recorded marker-based motion capture data from 10 males performing gait and shoulder abduction with and without external load. The primary findings were that the vertical ground reaction force during gait and the shoulder abduction/adduction angles, glenohumeral joint reaction forces and deltoideus forces during both shoulder abduction tasks showed comparable results. In addition, shoulder abduction/adduction range-of-motions were not significantly different between the two systems. However, the lower extremity joint angles, moments and reaction forces showed discrepancies during gait with correlations ranging from weak to strong, and for the majority of the variables, the marker-less system showed larger standard deviations. Although discrepancies between the systems were identified, the marker-less system shows potential, especially for tracking simple upper-body movements.

Keywords: *marker-less motion capture; Microsoft Kinect Sensor; iPi Motion Capture; ground reaction force prediction; musculoskeletal modelling; AnyBody Modeling System.*

Abbreviations:

Marker-based system (MBS)

Microsoft Kinect Sensor (MKS)

Range-of-motion (ROM)

Measured ground reaction force (MGRF)

Predicted ground reaction force (PGRF)

Marker-less system (MLS)

Physiological cross-sectional area (PCSA)

Unloaded shoulder abduction (SA)

Loaded shoulder abduction (LSA)

Ground reaction force (GRF)

AnyBody Modeling System (AMS)

Joint reaction force (JRF)

Pearson's correlation coefficient (r)

Root-mean-square deviation (RMSD)

1. Introduction

Motion capture is an important tool in various research areas and frequently used to collect kinematic input data for musculoskeletal models to estimate the muscle, joint and ligament forces [1-3]. One of the most commonly used motion capture methods is a combination of infrared cameras and skin markers [4].

Unfortunately, this method has limitations: 1) it is time consuming [5], 2) markers can become occluded [6], 3) marker-based systems (MBS) are complex and spacious [7] and 4) markers can move relative to the underlying bone, a phenomenon known as soft tissue artefact [8-9].

In recent years, the Microsoft Kinect Sensor (MKS) (Microsoft Corp., Redmond, WA, USA) has attracted the interest of researchers due to its potential application for motion analysis [5, 7, 10-15]. Originally developed to control gaming devices through gestures and voice commands, the MKS is a portable, easy-to-use, commercially available and significantly cheaper 3D motion capture system, compared to MBSS. For gesture recognition, the MKS combines an infrared laser projector and video camera to project a speckle pattern onto objects in its field-of-view, and creates a 3D map based on the recorded deformations in this pattern [7, 16]. Previous investigations of the MKS have shown encouraging results for the tracking of 3D marker coordinates [7], anatomical landmark positions and angular displacements [11], and shoulder abduction range-of-motion (ROM) [5]. However, the MKS only detects body segments directly in its field-of-view, which limits the sensor's application for tracking full-body movements, where body segments can obstruct each other. Recently developed software called iPi Motion Capture (iPi Soft, LLC, Moscow, Russia) is able to support two MKSs, which enables simultaneous tracking of all body segments. Additionally, a

previous investigation has demonstrated that the iPi software provides higher accuracy when tracking upper-body movements compared to freely available software [13]. If this system can provide accuracy comparable to a MBS, it would result in a compact and cheap motion capture system. However, two issues need to be addressed if the MKS is to be used in musculoskeletal modelling: firstly, the methodology for applying motion capture data obtained using the MKS, or a similar device, to drive musculoskeletal models does not currently exist and secondly, it is not possible to combine MKS and force plate data.

Therefore, the purpose of this investigation was to 1) develop a musculoskeletal model driven by marker-less motion capture data, obtained using two MKSs and iPi Motion Capture Software, without the use of force plates and 2) to evaluate the model's kinematic and kinetic outputs against those obtained when simultaneously recorded skin-marker trajectories with measured (MGRF) and predicted ground reaction forces (PGRF) were used as input to the model. This approach aimed at providing a framework for applying marker-less and force plate-less motion capture data as input to musculoskeletal models, in general, while validating the model outputs associated with the Kinect-based marker-less system (MLS) data.

2. Materials and methods

2.1 Experimental data

10 healthy males (age 23.50 ± 1.27 years, height 181.60 ± 4.40 cm, weight 76.12 ± 5.26 kg) volunteered to participate in the investigation and provided written informed consent.

During data collection, participants only wore tight fitting underwear or shorts, which enabled the placement of markers on the body as well as allowing the MLS to distinguish body segments. The following movements were executed: 1) gait at a self-selected pace, 2) unloaded shoulder abduction (SA) and 3) loaded shoulder abduction (LSA). These movements were chosen in order to determine the MLS's ability for tracking both full-body and isolated upper-body movements. Furthermore, the inclusion of both loaded and unloaded shoulder abduction enabled evaluation of the model's kinetic output in response to different loading conditions. Participants were instructed to walk at their self-selected pace and completed five gait trials. Likewise, five trials were completed for each of the two shoulder abduction tasks, each consisting of three consecutive repetitions. For the SA and LSA trials, participants were instructed to raise their dominant arm to an approximately horizontal position with and without a three kg dumbbell held in their hand, respectively. One repetition was completed when the participants returned their arm to its starting position along the torso. Four successful trials of each movement were selected for further analysis, as data from single trials for a number of participants were incomplete due to either marker occlusion more than 10% or incomplete movement reconstruction in the iPi software. For test subjects where all trials were successful, we excluded the first collected trial.

Data were simultaneously collected using the MLS and MBS. The MLS consisted of two MKSs, sampling at 30 Hz, and the recordings were processed using iPi Recorder v. 2.2.2.27 (iPi Soft LLC, Moscow, Russia). The MKSs were positioned 4.7 m from each other, elevated 1 m from the ground with an angle of 86.5 degrees between the sensors' field-of-views, which resulted in a distance of approximately 3.4 m from the sensors to the center of the measurement volume. 33 passive reflective markers were placed on the participants using a full-body

protocol and their trajectories tracked using a MBS consisting of eight infrared high-speed cameras (Oqus 300 series), sampling at 100 Hz, combined with Qualisys Track Manager v. 2.7 (Qualisys, Sweden). Ground reaction forces (GRF) were obtained at 2000 Hz using three force plates (AMTI, MA, USA).

2.2 Computational methods

2.2.1 Full-body model

The musculoskeletal models were developed using the Anybody Modeling System (AMS) v. 6.0.2 (AnyBody Technology A/S, Aalborg, Denmark) based on the *GaitFullBody* template from the AnyBody Managed Model Repository v. 1.5, in which the lower extremity model is based on the cadaver dataset collected by Horsman et al. [17], the lumbar spine model based on the work of de Zee et al. [18] and the shoulder and arm model based on the work of the Delft Shoulder Group [19-21]. For each trial, two musculoskeletal models were created: one driven by the marker-less motion capture data and one by the marker-based data. The steps included in the two modelling procedures are illustrated in Fig. 1.

2.2.2 Geometric and inertial parameter scaling

In order to scale the cadaver-based model to the different sizes of the subjects, a length-mass-scaling law [22] was applied, which utilize the segment lengths as predictor. These segment lengths were estimated differently between the two models as will be explained later.

The total body mass was distributed to the individual segments using the regression equations of Winter et al. [23]. Geometric scaling of each segment was accomplished by introducing a linear diagonal scaling matrix that was applied to each point on the segment, including the geometric center-of-masses. The entry of

the scaling matrix for the longitudinal direction was computed as the ratio between the unscaled and scaled segment lengths. In the two other orthogonal directions, the scaling was computed as the square root of the mass ratios divided by the length ratios between the scaled and unscaled models [22].

For estimation of the mass moments of inertia, the segments were assumed cylindrical with a uniform density, with the length and mass equal to the segment length and mass.

2.2.3 Muscle recruitment problem

The muscle recruitment problem was solved by formulating a polynomial optimization problem that minimizes a scalar objective function, G , subject to the dynamic equilibrium equations and non-negativity constraints, ensuring that the muscles can only pull and that the muscle forces do not exceed the strength of the muscles:

$$\min_{\mathbf{f}} G(\mathbf{f}^M) = \sum_{i=1}^{n^{(M)}} A_i \left(\frac{f_i^{(M)}}{N_i} \right)^3 \quad (1)$$

$$\mathbf{C}\mathbf{f} = \mathbf{d}$$

$$0 \leq f_i^{(M)} \leq N_i, \quad i = 1, \dots, n^{(M)}.$$

\mathbf{M} indicates the muscle forces, $f_i^{(M)}$ is the i th muscle force, $n^{(M)}$ is the number of muscles and N_i is the strength of the muscle. \mathbf{C} is the coefficient matrix for the dynamic equilibrium equations, \mathbf{f} is a vector of unknown muscle and joint reaction forces and \mathbf{d} contains all external loads and inertia forces. Finally, A_i is the physiological cross-sectional area (PCSA) of each muscle unit and, for split muscles, each unit was assigned the corresponding fraction of the total muscle PCSA, resulting from a uniform subdivision by the number of units. Further

details about muscle recruitment can be found in Damsgaard et al. [24] and Marra et al. [25].

The strength of the muscles were assumed to be constant, independent of the muscle length and contraction velocity, with the strength set to the values reported in the data sets for the different body parts. Furthermore, the muscle strengths were adjusted using a strength scaling factor based on fat percentage [22]. The fat percentage was estimated from each subject's Body-Mass-Index, which was determined using the regression equation for men reported by Frankenfield et al. [26].

In both models, muscles were added to the lower extremities. For the shoulder abduction trials, additional muscles were added to the torso, shoulder and arm. The dumbbell weight, associated with the LSA, was modelled as a downward vertical vector applying a force of 29.4 N at the palm of the hand.

2.2.4 Musculoskeletal model driven by the marker-less data

Data obtained using the MLS were processed in iPi Mocap Studio v. 2.5.1.159 (iPi Soft, LLC, Moscow, Russia), which fitted a 19-segment stick figure to each frame in the depth data generated by the MKSs. The stick figure was exported from iPi Mocap Studio and imported into AMS together with the *GaitFullBody* model.

The *GaitFullBody* model was set up to automatically scale the segment lengths according to the joint-to-joint distances of the stick figure. The segment lengths in the musculoskeletal model that could be directly computed from the stick figure were scaled based on joint-to-joint distances, as for instance the pelvis width (hip-to-hip joint center distance). For the trunk, hands and feet, however, the segment lengths were not directly obtainable from the stick figure. Therefore,

an additional step was introduced in order to scale these segments in the model. First, additional nodes were added to the musculoskeletal model at locations corresponding to points identifiable on the stick figure. Second, the unscaled model was placed in a neutral position and the distance between the added nodes were computed and saved together with the unscaled segment lengths. Subsequently, the ratio between the unscaled segment lengths and the nodes was multiplied onto the segment length measurements on the stick figure before being used to scale the respective segments in the musculoskeletal model.

To obtain tracking of the stick figure by the musculoskeletal model, virtual markers were introduced on both the stick figure and the musculoskeletal model. On the stick figure, virtual markers were located around anatomical landmarks that were possible to define on both the stick figure and the musculoskeletal model (further details are provided as supplementary material). Based on these virtual markers, a nonlinear least-square optimization problem was defined that minimized the least-square difference between the virtual markers on the stick figure and those on the musculoskeletal model. This optimization problem was solved using the method of Andersen et al. [27]. This tracking ensured that the musculoskeletal model optimally tracked the stick figure even though the two models differed in segment and joint definitions. Due to the lack of measurements of subtalar eversion and neck flexion, these were fixed in neutral positions.

Since GRFs were not measured by the MLS, these were predicted by the model based on measured full-body kinematic data only. This was enabled by introducing artificial muscle-like actuators at 12 contact nodes defined under each foot. To overcome the underdeterminacy issue during double support, the computation of the GRFs was made part of the muscle recruitment algorithm. Five unidirectional actuators were added to each contact node, which combined

were able to generate a normal force perpendicular to the laboratory floor and static friction forces (with a friction coefficient of 0.5) in the medio-lateral and anterior-posterior directions. Ground contact was defined as established when the node was within 50 mm of the ground plane and the velocity of the node relative to the ground was below 1.3 m/s. The transition from no contact to full contact condition was smoothed similarly to the procedures of Skals et al. [28] using the velocity of the nodes. Further details and validation of the method for an array of activities of daily living and sports-related movements were provided in Fluit et al. [29] and Skals et al. [28], respectively.

2.2.5 Musculoskeletal model driven by the marker-based data

For the models driven by the marker-based data, the model scaling and kinematic analysis were performed using the optimization methods of Andersen et al. [8, 27]. Firstly, for each subject, the model segment lengths and model marker positions were estimated by minimizing the least-square difference between model and experimental markers using the method of Andersen et al. [8] for a selected gait trial. These segment lengths and marker positions were subsequently saved and used for the analysis of all other trials. Secondly, the optimized segment lengths and marker positions were loaded and the least-square difference between model and experimental markers minimized to obtain the model kinematics [27]. Finally, two different versions of kinetic analysis were performed: one where the MGRFs were applied under the feet, and the muscle and joint reaction forces (JRF) computed using muscle recruitment [24], and one where the ground reaction forces were predicted similarly to the Kinect-based model (PGRF). Further details regarding the marker protocol and marker optimization procedure is provided as supplementary material.

2.3 Data Analysis

A complete gait cycle, i.e. from heel strike to heel strike, was analyzed for the gait trials. Shoulder abduction trials were analyzed from when the arm began its migration away from the torso until it returned to the initial position. For the gait trials, the following data were selected for analysis: vertical GRF, joint angles and moments for ankle plantar/dorsi flexion, knee flexion/extension, hip flexion/extension, abduction/adduction and internal/external rotation, resultant JRFs for the ankle, knee and hip, and muscle forces for the gastrocnemius, vasti and glutei. To account for the fact that the muscles were split into multiple branches in the models, the average force across all muscle branches were used in the analysis. In addition, peak resultant JRFs, peak vertical GRF, peak muscle forces and joint ROMs were computed. For the shoulder abduction trials, the following data were selected for analysis: shoulder flexion/extension, abduction/adduction and internal/external rotation angles and moments, resultant glenohumeral JRF, muscle force for the deltoideus, peak resultant glenohumeral JRF, deltoideus peak force and joint ROMs.

To compare the variables, Pearson's correlation coefficient (r) and root-mean-square deviation (RMSD) were computed for each trial separately and presented as the mean \pm 1 SD. The absolute values of r were categorized as weak, moderate, strong and excellent for $r \leq 0.35$, $0.35 < r \leq 0.67$, $0.67 < r \leq 0.90$ and $0.90 < r$, respectively [30]. The Friedman test was applied to statistically compare the peak vertical GRFs, peak resultant JRFs, peak muscle forces and ROMs between the three methods, and Wilcoxon paired-sample tests were used for post-hoc analysis if significant differences were found between the three groups. To account for multiple testing, a Bonferroni correction was implemented for the

Friedman test and significant differences are only reported for $p < 0.05/11 = 0.0045$. Joint moments and all forces are expressed as percentage of bodyweight times height (% BW x BH) and percentage of bodyweight (% BW), respectively.

3. Results

The time-histories of the selected variables for the gait and shoulder abduction trials are depicted in Figs. 2-4 and 5-7, respectively. Correlation coefficients and RMSDs are listed in Tables 1(a-c) for gait and Table 2 for the shoulder abduction trials. The results of the Wilcoxon signed-rank tests are summarized in Tables 3(a-c). The Friedman test showed significant differences between the three methods for all peak forces ($p \leq 0.0045$) with the exception of the SA glenohumeral peak resultant JRF ($p = 0.6077$), and the Wilcoxon signed-rank test was, therefore, applied as post-hoc analysis for the remaining variables.

Comparable results were found between the MBS with MGRFs and PGRFs for all analyzed variables (see Table 1(b)) with correlations ranging from 0.77 (hip internal/external rotation moment) to 0.94 (knee and hip resultant JRF), and RMSDs ranging from 0.50 ± 0.11 (hip internal/external rotation moment) to 56.60 ± 12.57 (ankle resultant JRF). Furthermore, the shape and magnitude differences between the two methods and the MLS were almost identical, so in the following, only the comparisons between the MBS with MGRF and the MLS are summarized. It should be noted, however, that the Wilcoxon signed-rank test showed significant differences between the two methods for all peak forces (see Table 3(b)) with the exception of the peak vertical GRF (mean diff. = -0.72 ± 3.72 , $p = 0.2477$).

When comparing the MBS and MLS, similar results were found for the shoulder abduction/adduction angles, glenohumeral resultant JRFs and deltoideus

forces during both shoulder abduction tasks, the shoulder flexion/extension and abduction/adduction moments during LSA, and the vertical GRF during gait. However, the MLS's tracking of the lower body during gait showed discrepancies compared to the MBS and was, in general, inconsistent with correlations ranging from -0.63 (hip internal/external rotation angle) to 0.82 (hip flexion/extension angle) (see Table 1(a)). The Wilcoxon paired-sample tests (see Table 3(a)) showed significant differences for the ankle plantar/dorsi flexion ROM ($p < 0.0001$), knee ($p < 0.0001$) and hip flexion/extension ROM ($p < 0.0001$), peak vertical GRF ($p < 0.0001$), knee ($p < 0.0001$) and hip peak resultant JRF ($p < 0.0001$), and glutei peak force ($p < 0.0001$) during gait. For the shoulder abduction tasks, significant differences were found for the SA shoulder internal/external rotation ROM ($p = 0.0044$), LSA glenohumeral peak resultant JRF ($p < 0.0001$) and deltoideus peak force ($p < 0.0001$).

3.1 Gait

Strong correlations were found between the systems for the vertical GRF (0.85), knee flexion/extension angle (0.81), hip flexion/extension angle (0.82) and abduction/adduction angle (0.81), ankle plantar/dorsi flexion (0.71) and hip abduction/adduction moment (0.77), ankle (0.80), knee (0.78) and hip (0.71) resultant JRFs, and glutei force (0.77). However, the other variables showed correlations ranging from weak to moderate with the hip internal/external rotation angle (-0.63) and moment (0.57) showing the outermost values. No significant differences were found for the hip abduction/adduction ROM ($p = 0.1704$) and internal/external rotation ROM ($p = 0.0983$), ankle peak resultant JRF ($p = 0.4356$), gastrocnemius ($p = 0.1222$) and vasti peak force ($p = 0.5633$).

3.2 Shoulder abduction

For the SA trials, strong correlations were established for the shoulder abduction/adduction angle (0.89) and internal/external rotation angle (0.68), and no significant differences were found for the shoulder flexion/extension ROM ($p = 0.4046$), abduction/adduction ROM ($p = 0.7572$), glenohumeral peak resultant JRF and deltoideus peak force ($p = 0.0099$). LSA showed excellent correlations for the shoulder abduction/adduction angle (0.96) and moment (0.90), while strong correlations were found for the shoulder internal/external rotation angle (0.72), glenohumeral resultant JRF (0.87) and deltoideus force (0.88). No significant differences were found for the shoulder flexion/extension ($p = 0.1322$), abduction/adduction ($p = 0.5364$) and internal/external rotation ROM ($p = 0.4436$).

4. Discussion

We developed a musculoskeletal model driven by motion capture data obtained using a MLS, consisting of dual MKSs and iPi Motion Capture software, and evaluated the model outputs against those obtained from musculoskeletal models driven by simultaneously recorded skin marker trajectories. Furthermore, to enable kinetic analysis with the MLS, the GRF&Ms were predicted by incorporating the method of Fluit et al. [29] and Skals et al [28]. The developed methodology enabled, for the first time, estimation of kinetic variables based on a MLS. In general, the motion variables compared between the systems revealed different results for the studied movements. The vertical GRF data showed a strong correlation during gait, but the peak values were significantly different and the time of occurrence in the gait cycles deviated slightly. Noticeable

discrepancies were observed for the remaining variables during gait, which, however, were inconsistent. Shoulder abduction/adduction angles showed strong to excellent correlations and the ROMs were not significantly different during both SA and LSA. For the LSA, strong to excellent correlations were also found for the shoulder abduction/adduction moment, glenohumeral resultant JRF and deltoideus force, but the peak forces were, however, significantly different. Although the results for the MLS were generally associated with larger standard deviations than the MBS, the shoulder abduction measurements showed considerably lower standard deviations compared to the results for the lower body.

Joint angles and ROM showed poor agreement during gait, most noticeably in the tracking of the ankle plantar/dorsi flexion and hip internal/external rotation angles. The large discrepancies associated with the ankle angles could also have contributed to the discrepancies for the knee and hip angles between the systems, due to the joint constraints enforced by the model. The MLS's tracking of ankle plantar/dorsi flexion was associated with large errors and a significant difference between the systems was observed for the ankle plantar/dorsi flexion ROM. It was assessed that these tracking errors were mainly associated with three issues. Firstly, the tracking of the ankle could have been compromised as a result of light reflected on the ground during data collection. Light sensitivity has been proposed as a limitation of the MKS [7], which could substantially reduce the applicability of the MLS outside a controlled environment. Secondly, Dutta et al. [7] reported that tracking errors of the MKS were considerably larger near the edges of the sensor's field-of-view, which could have caused the poor tracking of the participants' feet in the current investigation. This is very likely since the MKS was developed to control gaming devices

mainly through hand gestures, which makes the depth information near the edges of the sensor's field-of-view less important for its primary application. Thirdly, due to the close proximity of the feet and the ground during the stance phase of gait, a clear distinction between the feet and ground does not exist in the depth map recorded by the MKSs, which may cause inaccuracies when fitting the stick figure to the depth data.

The differences between the results for the upper-body and lower-body variables could be partially explained by the argumentation above. In addition, the higher tracking accuracy for the shoulder abduction tasks could be the result of a combination of two factors: 1) the movement occurs in the center of the sensor's field-of-view, where the tracking error is presumably lowest, and 2) the clear visibility of the arm movement during this task compared to e.g. the legs during gait. The importance of the visibility of the movements is clear when comparing the shoulder abduction/adduction angles to the flexion/extension and internal/external rotation angles, which also showed poor agreement. Bonnechère et al. [5] reported comparable accuracy between a MLS, consisting of a single MKS and the proprietary software, and a MBS for tracking shoulder abduction, but found poor to no agreement between the systems for hip abduction and knee flexion. The application of two MKS and a more complex stick figure model, associated with the iPi software, was not able to address this limitation and could not provide tracking accuracy of the lower body comparable to the MBS, hereby, supporting these results.

In general, the kinetic variables for the shoulder abduction tasks showed encouraging results, particularly for the glenohumeral resultant JRFs and deltoideus forces, whereas the results for the lower extremities were less accurate. When the external load was applied to the shoulder abduction task, however, the

variation in the kinetic variables increased noticeably, which indicates that the Kinect-based model does not respond well to increases in loading conditions. Strong correlations were observed for the ankle, knee and hip resultant JRFs as well as the glutei force during gait, while the gastrocnemius and vasti forces differed considerably. The ankle and knee resultant JRFs showed similarities in magnitude between the systems, but the timing of the movement differed slightly. Conversely, the hip resultant JRF differed considerably in magnitude, and the peak forces were overestimated compared to the results of the marker-based models. For the kinetic variables, the most encouraging results were found for the vertical GRF, which showed a strong correlation between the systems. Although the peak forces differed slightly in magnitude and timing, the overall similarity between the predicted and measured GRFs supports the results of previous validation studies [28, 29], showing that predicted GRFs are comparable to those measured using force plates.

With regards to the practical usability of the MLS, limitations were identified. Firstly, the volume in which movement could be tracked was restricted, which required careful positioning of the two MKSs to enable tracking of a single gait cycle. Secondly, any alteration in the background required recalibration of the system, which additionally complicates data collection. Thirdly, since the automatic tracking by the iPi software utilizes the solution of the previous frame as the initial guess for fitting the stick figure to the current frame, a large movement from one frame to the next could cause the process to fail. To overcome this, manual improvements of the initial guess for these frames were required. Although this did not affect the estimated stick figure movements, it was a time consuming task that must be overcome before the system can be used on a larger scale. Finally, in regards to the MLS's use in musculoskeletal modelling,

the inability of the MLS for determining the relative position of the force plates to the MKSs required the implementation of GRF prediction. Although the PGRFs were overall similar to the MGRFs, this limitation could have implications due to the MLS's poor tracking of the feet, since it can potentially be challenging to accurately determine when foot-ground contact is established.

During data collection, additional functional trials were collected, but these were later excluded due to largely inaccurate movement reconstruction in iPi; the excluded movements were counter-movement jump and forward lunge. For the counter-movement jump trials, large errors were observed during movement reconstruction, particularly for the lower body, which caused the procedure to fail completely. It was simply not possible to obtain accurate kinematics for this high-velocity movement due to the relatively low sampling frequency of the MLS (30 Hz). The lunge trials were successfully reconstructed, but the results were associated with large errors, mainly caused by a very poor tracking of the ankle flexion/extension angle. Because of the joint constraints imposed by the musculoskeletal model, this error additionally caused poor reconstruction of the knee flexion/extension angle. Hence, large discrepancies were observed between the two systems for all variables associated with the ankle and knee. As similar tendencies were observed during gait, we assessed that the forward lunge trials did not provide additional meaningful information to the investigation.

This study contains a number of limitations. First, we used a MBS for validation. MBSs are associated with limitations regarding their accuracy, especially due to soft tissue artefacts, and do not possess the accuracy of a golden standard such as bone pins [31] or 3D fluoroscopy [32]. However, the differences observed for instance in knee flexion/extension angles in the present investigation

exceed the associated differences between MBSs and bone pins reported by Benoit et al. [31]. In addition, the application of bone pins or 3D fluoroscopy would have been unsuitable, as the investigation aimed at assessing the MLS's ability to track full-body motion. Although the MBS is associated with limitations, it would be a valuable result to establish comparable accuracy between the MLS and MBS, especially due to the portability and low price of the MLS.

Second, retro-reflective skin markers were attached to the subjects during the data acquisition with the MKSs. Since these markers reflect infrared light, they affect the light measured by the MKSs and, consequently, the estimated depth map. Although the influence of the markers was not specifically investigated, we did not observe any noticeable effect in the depth maps and we anticipate that the effect is either minor or negligible. It would, however, be worth investigating this effect in a future study.

Third, since the stick figure and musculoskeletal models have slightly different joint constraint definitions, the applied tracking approach results in an imperfect tracking of the stick figure and hence, the resulting movement of the musculoskeletal model may deviate from the depth measurements. To overcome this, future research should explore direct tracking of the depth map by the musculoskeletal model applying for instance a similar approach as proposed by Sandau et al. [33].

In summary, the results for the vertical GRF, shoulder abduction/adduction angles and ROMs, glenohumeral resultant JRFs and deltoideus forces were encouraging, but the MLS revealed limitations, particularly for tracking the lower body. Considering these results, the MLS could be applied to track simple upper-body movements, and further development of this

technology towards its application in motion analysis seems warranted, as the MLS provides a portable and significantly cheaper (< 1000 USD) solution compared to MBSs. Therefore, future work should focus on assessing the ability of the system to track other simple upper body movements relevant for diagnostics and ergonomics.

5. References

1. Mellon, S.J., Grammatopoulos, G., Andersen, M.S., Pegg, E.C., Pandit, H.G., Murray, D.W., Gill, H.S.: Individual motion patterns during gait and sit-to-stand contribute to edge-loading risk in metal-on-metal hip resurfacing. *P. I. Mech. Eng. H.* **227**, 799-810 (2013)
2. Alkjær, T., Wieland, M.R., Andersen, M.S., Simonsen, E.B., Rasmussen, J.: Computational modeling of a forward lunge: towards a better understanding of the function of the cruciate ligaments. *J. Anat.* **221**, 590-597 (2012)
3. Weber, T., Dendorfer, S., Dullien, S., Grifka, J., Verkerke, G.J., Renkawitz, T.: Measuring functional outcome after total hip replacement with subject-specific hip joint loading. *P. I. Mech. Eng. H.* **226**, 939-946 (2012)
4. Cappozzo, A., Della Croce, U., Leardini, A., Chiari, L.: Human movement analysis using stereophotogrammetry. Part 1: theoretical background. *Gait Posture* **21**, 186–196 (2005)
5. Bonnechère, B., Jansen, B., Salvia, P., Bouzahouene, H., Omelina, L., Moiseev, F., Sholukha, V., Cornelis, J., Rooze, M., Van Sint Jan, S.: Validity and reliability of the Kinect within functional assessment activities: comparison with standard stereophotogrammetry. *Gait Posture* **39**, 593–598 (2014)

6. Herda, L., Fua, P., Plänkers, R., Boulic, R., Thalmann, D.: Using skeleton-based tracking to increase the reliability of optical motion capture. *Hum. Movement Sci.* **20**, 313-341 (2001)
7. Dutta, T.: Evaluation of the KinectTM sensor for 3-D kinematic measurement in the workplace. *Appl. Ergon.* **43**, 645–649 (2012)
8. Andersen, M.S., Damsgaard, M., MacWilliams, B., Rasmussen, J.: A computationally efficient optimisation-based method for parameter identification of kinematically determinate and over-determinate biomechanical systems. *Comput. Methods Biomech. Biomed. Engin.* **13**, 171–183 (2010)
9. Stagni, R., Fantozzi, S., Capello, A., Leardini, A.: Quantification of soft tissue artefact in motion analysis by combining 3D fluoroscopy and stereophotogrammetry: a study on two subjects. *Clin. Biomech.* **20**, 320-329 (2005)
10. Clark, R.A., Pua, Y.-H., Fortin, K., Ritchie, C., Webster, K.E., Denehy, L., Bryant, A.L.: Validity of the Microsoft Kinect for assessment of postural control. *Gait Posture* **36**, 372–377 (2012)
11. Clark, R.A., Bower, K.J., Mentiplay, B.F., Paterson, K., Pua, Y.-H.: Concurrent validity of the Microsoft Kinect for assessment of spatiotemporal gait variables. *J. Biomech.* **46**, 2722–2725 (2013a)
12. Clark, R.A., Pua, Y.-H., Bryant, A.L., Hunt, M.A.: Validity of the Microsoft Kinect for providing lateral trunk lean feedback during gait retraining. *Gait Posture* **38**, 1064–1066 (2013b)
13. Choppin, S., Wheat, J.: Marker-less tracking of human movement using Microsoft Kinect. In: Bradshaw, E.J., Burnett, A., Hume, P.A. (ed.) *Proceedings of the 30th Annual Conference of Biomechanics in Sports*, Melbourne, 2012

14. Oikonomidis, I., Kyriazis, N., Argyros, A.A.: Efficient model-based 3D tracking of hand articulations using Kinect. In: Hoey, J., McKenna, S., Trucco, E. (ed.) Proceedings of the 22nd British Machine Vision Conference, Dundee, 2011
15. Xia, L., Chen, C.-C., Aggarwal, J.K.: Human detection using depth information by Kinect. In: Computer Vision and Pattern Recognition Workshops (CVPRW), 2011 IEEE Computer Society Conference on, Colorado Springs, CO (US), 20-25 June 2011
16. Khoshelham, K., Elberink, S.O.: Accuracy and resolution of Kinect depth data for indoor mapping applications. *Sensors* **12**, 1437-1454 (2012)
17. Horsman, M.D.K., Koopman, H.F.J.M., van der Helm, F.C.T., Prosé, L.P., Veeger, H.E.J.: Morphological muscle and joint parameters for musculoskeletal modelling of the lower extremity. *Clin. Biomech.* **22**, 239–247 (2007)
18. de Zee, M., Hansen, L., Wong, C., Rasmussen, J., Simonsen, E.B.: A generic detailed rigid-body lumbar spine model. *J. Biomech.* **40**, 1219-1227 (2007)
19. Veeger, H.E.J., van der Helm, F.C.T., van der Woude, L.H.V., Pronk, G.M., Rozendal, R.H.: Inertia and muscle contraction parameters for musculoskeletal modelling of the shoulder mechanism. *J. Biomech.* **24**, 615-629 (1991)
20. Veeger, H.E.J., Yu, B., An, K.-N., Rozendal, R.H.: Parameters for modeling the upper extremity. *J. Biomech.* **30**, 647-652 (1997)
21. Van der Helm, F.C., Veeger, H.E., Pronk, G.E., Van der Woude, L.H., Rozendal, R.H.: Geometry parameters for musculoskeletal modeling of the shoulder system. *J. Biomech.* **25**, 129-144 (1992)
22. Rasmussen, J., de Zee, M., Damsgaard, M., Christensen, S.T., Marek, C., Siebertz, K.: A general method for scaling musculoskeletal models. In: Proceedings of the 10th International Symposium on Computer Simulation in Biomechanics, Cleveland, OH (US), 28-30 July, 2005

23. Winter, D.A.: Biomechanics and Motor Control of Human Movement. John Wiley & Sons, Hoboken, New Jersey (2005)
24. Damsgaard, M., Rasmussen, J., Christensen, S.T., Surma, E., de Zee, M.: Analysis of musculoskeletal systems in the AnyBody Modeling System. *Simul. Model. Pract. Th.* **14**, 1100-1111 (2006)
25. Marra, M.A., Vanheule, V., Fluit, R., Koopman, B.H.F.J.M., Rasmussen, J., Verdonchot, N., Andersen, M.S.: A subject-specific musculoskeletal modeling framework to predict in vivo mechanics of total knee arthroplasty. *J. Biomech. Eng.* **137**, 020904 (2015)
26. Frankenfield, D.C., Rowe, W.A., Cooney, R.N., Smith, J.S., Becker, D.: Limits of body mass index to detect obesity and predict body composition. *Nutrition* **17**, 26-30 (2001)
27. Andersen, M.S., Damsgaard, M., Rasmussen, J.: Kinematic analysis of over-determinate biomechanical systems. *Comput. Methods Biomech. Biomed. Engin.* **12**, 371–384 (2009)
28. Skals, S., Jung, M.K., Damsgaard, M., Andersen, M.S.: Prediction of ground reaction forces and moments during sports-related movements. *Multibody Syst. Dyn.*, 1-21 (2016)
29. Fluit, R., Andersen, M.S., Kolk, S., Verdonchot, N., Koopman, H.F.J.M.: Prediction of ground reaction forces and moments during various activities of daily living. *J. Biomech.* **47**, 2321-2329 (2014)
30. Taylor, R.: Interpretation of the correlation coefficient: a basic review. *J. Diagn. Med. Sonog.* **6**(1), 35-39 (1990)
31. Benoit, D.L., Ramsey, D.K., Lamontagne, M., Xu, L., Wretenberg, P., Renström, P.: Effect of skin movement artifact on knee kinematics during gait and cutting motions measured in vivo. *Gait Posture* **24**, 152–164 (2006)

32. Barre, A., Thiran, J.-P., Jolles, B.M., Theumann, N., Aminian, K.: Soft tissue artifact assessment during treadmill walking in subjects with total knee arthroplasty. *IEEE Trans. Biomed. Eng.* **60**, 3131–3140 (2013)
33. Sandau, M., Koblauch, H., Moeslund, T.B., Aanæs, H., Alkjær, T., Simonsen, E.B.: Markerless motion capture can provide reliable 3D gait kinematics in the sagittal and frontal plane. *Med. Eng. Phys.* **36**, 1168-1175 (2014)

Accepted Manuscript

Table 1(a) - Correlation and RMSD between the marker-based system with MGRFs and MLS for the selected variables during gait. The results are presented as the mean and standard deviation over the subjects.

MBS (MGRF) vs. MLS		
Gait		
Variable	Mean $r \pm SD$	RMSD $\pm SD$
Ankle plantar/dorsi flexion angle (deg)	0.57 ± 0.17	14.83 ± 4.47
Knee flexion/extension angle (deg)	0.81 ± 0.13	11.08 ± 3.06
Hip flexion/extension angle (deg)	0.82 ± 0.18	15.20 ± 4.37
Hip abduction/adduction angle (deg)	0.81 ± 0.12	4.91 ± 1.18
Hip internal/external rotation angle (deg)	-0.63 ± 0.19	11.88 ± 3.48
Ankle plantar/dorsi flexion moment (% BW x BH)	0.72 ± 0.20	2.03 ± 0.77
Knee flexion/extension moment (% BW x BH)	-0.05 ± 0.32	2.11 ± 0.70
Hip flexion/extension moment (% BW x BH)	0.43 ± 0.30	1.99 ± 0.66
Hip abduction/adduction moment (% BW x BH)	0.77 ± 0.12	1.94 ± 0.50
Hip internal/external rotation moment (% BW x BH)	0.57 ± 0.20	0.75 ± 0.23
Vertical GRF (% BW)	0.85 ± 0.10	24.57 ± 8.88
Ankle resultant JRF (% BW)	0.80 ± 0.13	124.84 ± 44.98
Knee resultant JRF (% BW)	0.78 ± 0.10	92.49 ± 32.93
Hip resultant JRF (% BW)	0.71 ± 0.13	154.00 ± 69.13
Gastrocnemius (% BW)	0.50 ± 0.33	48.83 ± 18.60
Vasti (% BW)	0.06 ± 0.32	16.69 ± 7.67
Glutei (% BW)	0.77 ± 0.11	18.27 ± 5.80

Table 1(b) - Correlation and RMSD between the marker-based system with MGRFs and PGRFs for the selected variables during gait. The results are presented as the mean and standard deviation over the subjects.

MBS (MGRF) vs. MBS (PGRF)		
Gait		
Variable	Mean $r \pm SD$	RMSD $\pm SD$
Ankle plantar/dorsi flexion moment (% BW x BH)	0.93 ± 0.03	0.97 ± 0.15
Knee flexion/extension moment (% BW x BH)	0.80 ± 0.11	0.68 ± 0.11
Hip flexion/extension moment (% BW x BH)	0.86 ± 0.07	0.96 ± 0.22
Hip abduction/adduction moment (% BW x BH)	0.93 ± 0.02	0.69 ± 0.13
Hip internal/external rotation moment (% BW x BH)	0.77 ± 0.08	0.50 ± 0.11
Vertical GRF (% BW)	0.93 ± 0.03	16.48 ± 8.93
Ankle resultant JRF (% BW)	0.96 ± 0.02	56.60 ± 12.57
Knee resultant JRF (% BW)	0.94 ± 0.03	39.64 ± 6.42
Hip resultant JRF (% BW)	0.94 ± 0.03	40.31 ± 7.26
Gastrocnemius (% BW)	0.91 ± 0.05	20.66 ± 3.54
Vasti (% BW)	0.89 ± 0.13	4.53 ± 1.15
Glutei (% BW)	0.93 ± 0.03	6.69 ± 1.48

Table 1(c) - Correlation and RMSD between the marker-based system with PGRFs and MLS for the selected variables during gait. The results are presented as the mean and standard deviation over the subjects.

Variable	MBS (PGRF) vs. MLS	
	Gait	
Variable	Mean $r \pm SD$	RMSD $\pm SD$
Ankle plantar/dorsi flexion moment (% BW x BH)	0.71 ± 0.16	2.10 ± 0.66
Knee flexion/extension moment (% BW x BH)	-0.06 ± 0.37	1.88 ± 0.72
Hip flexion/extension moment (% BW x BH)	0.36 ± 0.32	2.82 ± 1.20
Hip abduction/adduction moment (% BW x BH)	0.73 ± 0.13	1.94 ± 0.50
Hip internal/external rotation moment (% BW x BH)	0.57 ± 0.15	0.78 ± 0.20
Vertical GRF (% BW)	0.82 ± 0.10	27.04 ± 8.44
Ankle resultant JRF (% BW)	0.77 ± 0.13	131.84 ± 45.06
Knee resultant JRF (% BW)	0.75 ± 0.11	96.86 ± 32.81
Hip resultant JRF (% BW)	0.71 ± 0.13	156.46 ± 69.18
Gastrocnemius (% BW)	0.48 ± 0.29	50.48 ± 18.20
Vasti (% BW)	0.06 ± 0.32	15.18 ± 7.50
Glutei (% BW)	0.73 ± 0.12	18.64 ± 5.74

Table 2 - Correlation and RMSD between the marker-based system with MGRFs and MLS for the selected variables during SA and LSA. The results are presented as the mean and standard deviation over the subjects.

MBS (MGRF) vs. MLS		
Shoulder abduction		
Variable	Mean $r \pm SD$	RMSD $\pm SD$
Shoulder flexion/extension angle (deg)	0.32 ± 0.38	10.74 ± 3.86
Shoulder abduction/adduction angle (deg)	0.89 ± 0.33	11.93 ± 13.57
Shoulder internal/external rotation angle (deg)	0.68 ± 0.39	32.75 ± 15.09
Shoulder flexion/extension moment (% BW x BH)	0.56 ± 0.22	0.06 ± 0.01
Shoulder abduction/adduction moment (% BW x BH)	0.66 ± 0.32	0.10 ± 0.05
Shoulder internal/external rotation moment (% BW x BH)	0.64 ± 0.30	0.07 ± 0.02
Glenohumeral resultant JRF (% BW)	0.62 ± 0.30	9.78 ± 4.95
Deltoides (% BW)	0.66 ± 0.33	2.88 ± 1.33
Loaded shoulder abduction		
Shoulder flexion/extension angle (deg)	0.52 ± 0.36	11.16 ± 13.68
Shoulder abduction/adduction angle (deg)	0.96 ± 0.16	9.07 ± 9.74
Shoulder internal/external rotation angle (deg)	0.72 ± 0.30	36.69 ± 12.89
Shoulder flexion/extension moment (% BW x BH)	0.56 ± 0.29	0.13 ± 0.04
Shoulder abduction/adduction moment (% BW x BH)	0.90 ± 0.38	0.18 ± 0.28
Shoulder internal/external rotation moment (% BW x BH)	0.54 ± 0.29	0.18 ± 0.06
Glenohumeral resultant JRF (% BW)	0.87 ± 0.37	20.63 ± 22.11
Deltoides (% BW)	0.88 ± 0.38	5.45 ± 6.16

Table 3(a) – Results of the Wilcoxon signed-rank test between the marked-based system with MGRFs and MLS, listing the p-value, mean difference and standard deviation for joint ROMs and peak forces. Significant differences are indicated with a * for $p < 0.0045$.

MBS (MGRF) vs. MLS		
Gait		
Variable	Mean diff. \pm SD	p-value
Ankle plantar/dorsi flexion ROM (deg)	30.16 ± 6.07	$< 0.0001^*$
Knee flexion/extension ROM (deg)	10.01 ± 5.00	$< 0.0001^*$
Hip flexion/extension ROM (deg)	8.62 ± 8.70	$< 0.0001^*$
Hip abduction/adduction ROM (deg)	-1.13 ± 4.05	0.1704
Hip internal/external rotation ROM (deg)	-1.38 ± 5.88	0.0983
Peak vertical GRF (% BW)	-8.47 ± 9.26	$< 0.0001^*$
Ankle peak resultant JRF (% BW)	7.77 ± 121.56	0.4356
Knee peak resultant JRF (% BW)	-129.69 ± 144.98	$< 0.0001^*$
Hip peak resultant JRF (% BW)	-387.10 ± 264.50	$< 0.0001^*$
Gastrocnemius peak force (% BW)	-12.02 ± 60.82	0.1222
Vasti peak force (% BW)	5.84 ± 30.30	0.5633
Glutei peak force (% BW)	-40.11 ± 24.16	$< 0.0001^*$
Shoulder abduction		
Shoulder flexion/extension ROM (deg)	0.19 ± 6.70	0.4046
Shoulder abduction/adduction ROM (deg)	2.60 ± 15.28	0.7572
Shoulder internal/external rotation ROM (deg)	6.41 ± 13.72	0.0044^*
Deltoides peak force (% BW)	-1.00 ± 2.98	0.0099
Loaded shoulder abduction		
Shoulder flexion/extension ROM (deg)	-0.73 ± 13.68	0.1322
Shoulder abduction/adduction ROM (deg)	-0.30 ± 4.83	0.5364
Shoulder internal/external rotation ROM (deg)	-1.80 ± 12.89	0.4436
Glenohumeral peak resultant JRF (% BW)	-21.96 ± 32.60	$< 0.0001^*$
Deltoides peak force (% BW)	-4.37 ± 7.11	$< 0.0001^*$

Table 3(b) - Results of the Wilcoxon signed-rank test between the marked-based system with MGRFs and PGRFs, listing the p-value, mean difference and standard deviation for joint ROMs and peak forces. Significant differences are indicated with a * for $p < 0.0045$.

MBS (MGRF) vs. MBS (PGRF)		
Gait		
Variable	Mean diff. \pm SD	p-value
Peak vertical GRF (% BW)	-0.72 ± 3.72	0.2477
Ankle peak resultant JRF (% BW)	-71.77 ± 49.87	$< 0.0001^*$
Knee peak resultant JRF (% BW)	-75.34 ± 46.26	$< 0.0001^*$
Hip peak resultant JRF (% BW)	-66.86 ± 50.98	$< 0.0001^*$
Gastrocnemius peak force (% BW)	-46.93 ± 24.07	$< 0.0001^*$
Vasti peak force (% BW)	5.64 ± 4.48	$< 0.0001^*$
Glutei peak force (% BW)	-4.38 ± 4.34	$< 0.0001^*$

Table 3(c) - Results of the Wilcoxon signed-rank test between the marked-based system with PGRFs and MLS, listing the p-value, mean difference and standard deviation for joint ROMs and peak forces. Significant differences are indicated with a * for $p < 0.0045$.

MBS (PGRF) vs. MLS		
Gait		
Variable	Mean diff. \pm SD	p-value
Peak vertical GRF (% BW)	-7.75 \pm 9.02	< 0.0001*
Ankle peak resultant JRF (% BW)	79.55 \pm 121.19	0.0004*
Knee peak resultant JRF (% BW)	-54.36 \pm 142.41	0.0599
Hip peak resultant JRF (% BW)	-320.25 \pm 263.98	< 0.0001*
Gastrocnemius peak force (% BW)	-34.92 \pm 55.83	0.0006*
Vasti peak force (% BW)	0.20 \pm 30.45	0.7881
Glutei peak force (% BW)	-35.73 \pm 24.12	< 0.0001*
Shoulder abduction		
Deltoideus peak force (% BW)	-1.00 \pm 2.98	0.0099
Loaded shoulder abduction		
Glenohumeral peak resultant JRF (% BW)	-113.14 \pm 36.71	< 0.0001*
Deltoideus peak force (% BW)	-33.81 \pm 8.75	< 0.0001*

Figure 1 –Top: marker-less data analysis workflow, where the data is 1) collected from two Microsoft Kinect Sensors using iPi Recorder, 2) tracked in iPi Mocap Studio, 3) the resulting stick figure is imported in AMS and tracked by a scaled musculoskeletal model, and 4) inverse dynamics, including prediction of ground reaction forces, is performed. Bottom: marker-based data analysis workflow, where the data is 1) collected with infrared cameras and force plates using Qualysis Track Manager, 2) imported into AMS for inverse kinematic analysis based on the marker trajectories and 3) kinetic analysis is performed with predicted and measured ground reaction forces.

Figure 2 – Results for gait, illustrating the ankle plantar/dorsi flexion angle (top left), knee (top centre) and hip flexion/extension angle (top right), ankle plantar/dorsi flexion moment (middle left), knee (middle centre) and hip flexion/extension moment (middle right), ankle (bottom left), knee (bottom centre) and hip resultant JRF (bottom right). The results for the marker-based system with MGRFs (red) and PGRFs (black), and marker-less system (blue) are illustrated as the mean \pm 1 SD (shaded area) over the subjects and trials.

Figure 3 – Results for gait, illustrating the hip abduction/adduction and internal/external rotation angles (top) and moments (bottom). The results for the marker-based system with MGRFs (red) and PGRFs (black), and marker-less system (blue) are illustrated as the mean \pm 1 SD (shaded area) over the subjects and trials.

Figure 4 – Results for gait, illustrating the vertical GRF (top left), gastrocnemius (top right), vasti (bottom left) and glutei force (bottom right). The results for the marker-based system with MGRFs (red) and PGRFs (black), and marker-less system (blue) are illustrated as the mean \pm 1 SD (shaded area) over the subjects and trials.

Figure 5 – Results for SA, illustrating the shoulder flexion/extension, abduction/adduction and internal/external rotation angles (top) and moments (bottom). The results for the marker-based

(red) and marker-less system (blue) are illustrated as the mean \pm 1 SD (shaded area) over the subjects and trials.

Figure 6 – Results for LSA, illustrating the shoulder flexion/extension, abduction/adduction and internal/external rotation angles (top) and moments (bottom). The results for the marker-based (red) and marker-less system (blue) are illustrated as the mean \pm 1 SD (shaded area) over the subjects and trials.

Figure 7 – Results for SA (left) and LSA (right), illustrating the glenohumeral resultant JRF (top) and deltoideus force (bottom). The results for the marker-based (red) and marker-less system (blue) are illustrated as the mean \pm 1 SD (shaded area) over the subjects and trials.

Figure 1

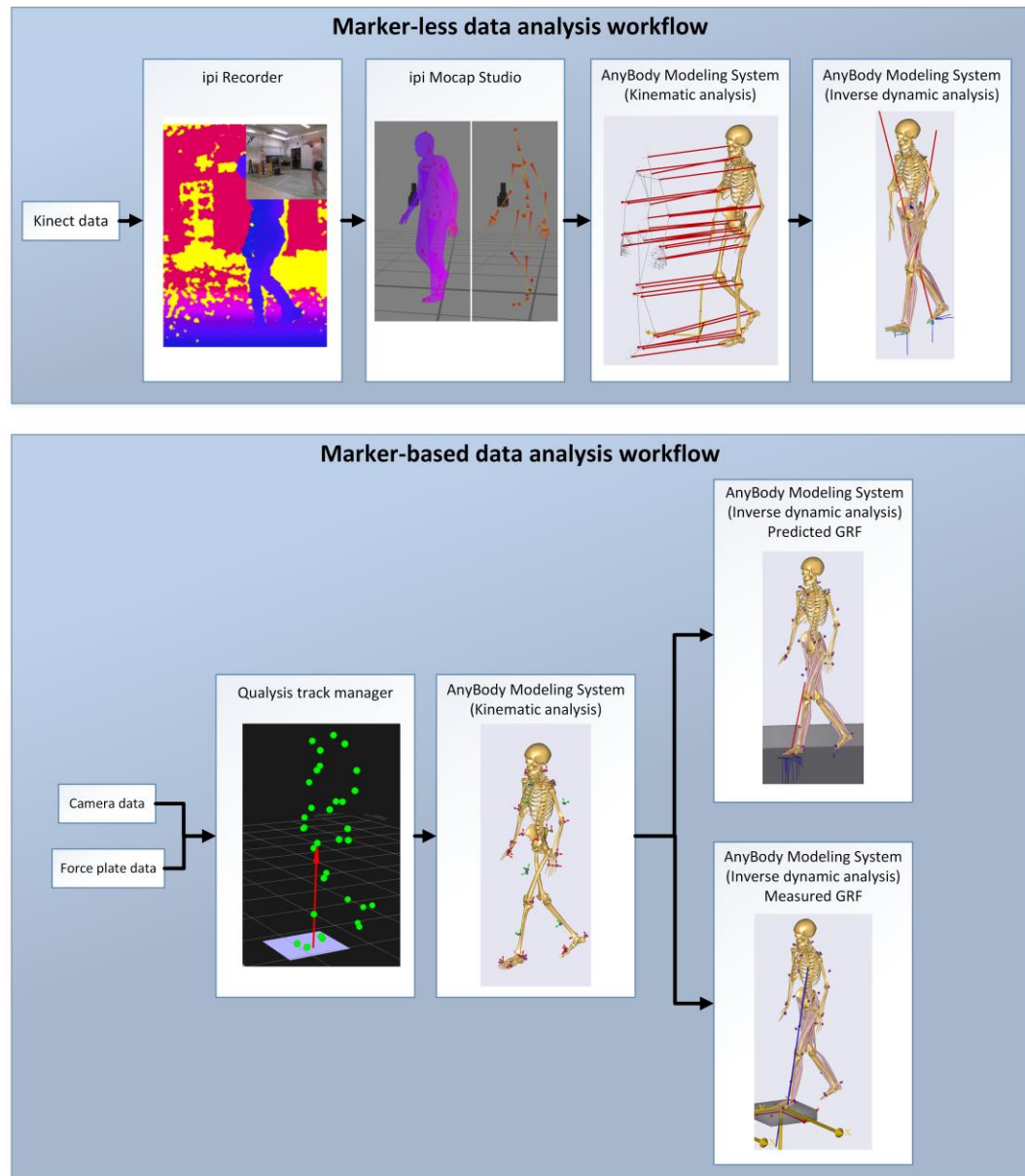


Figure 2

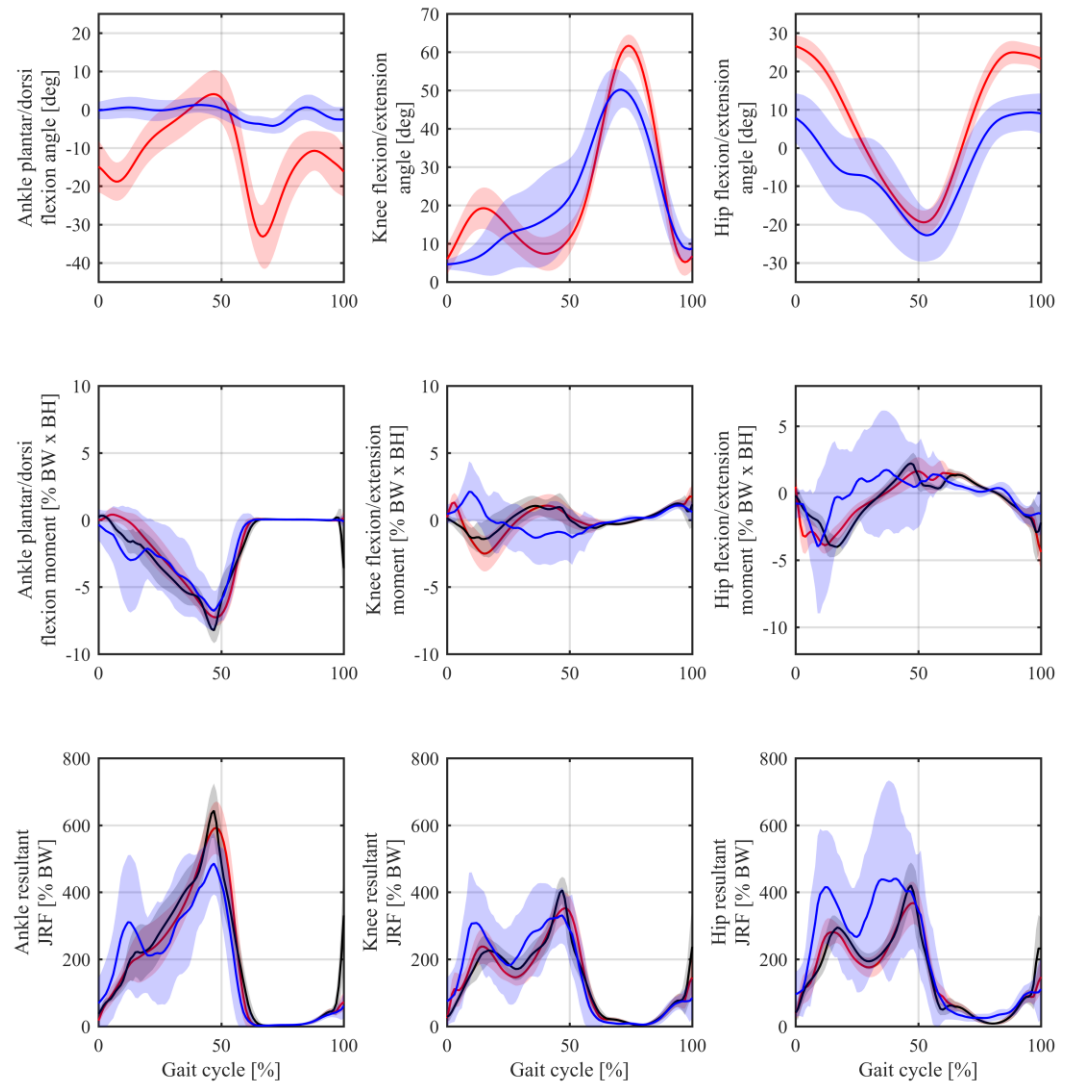


Figure 3

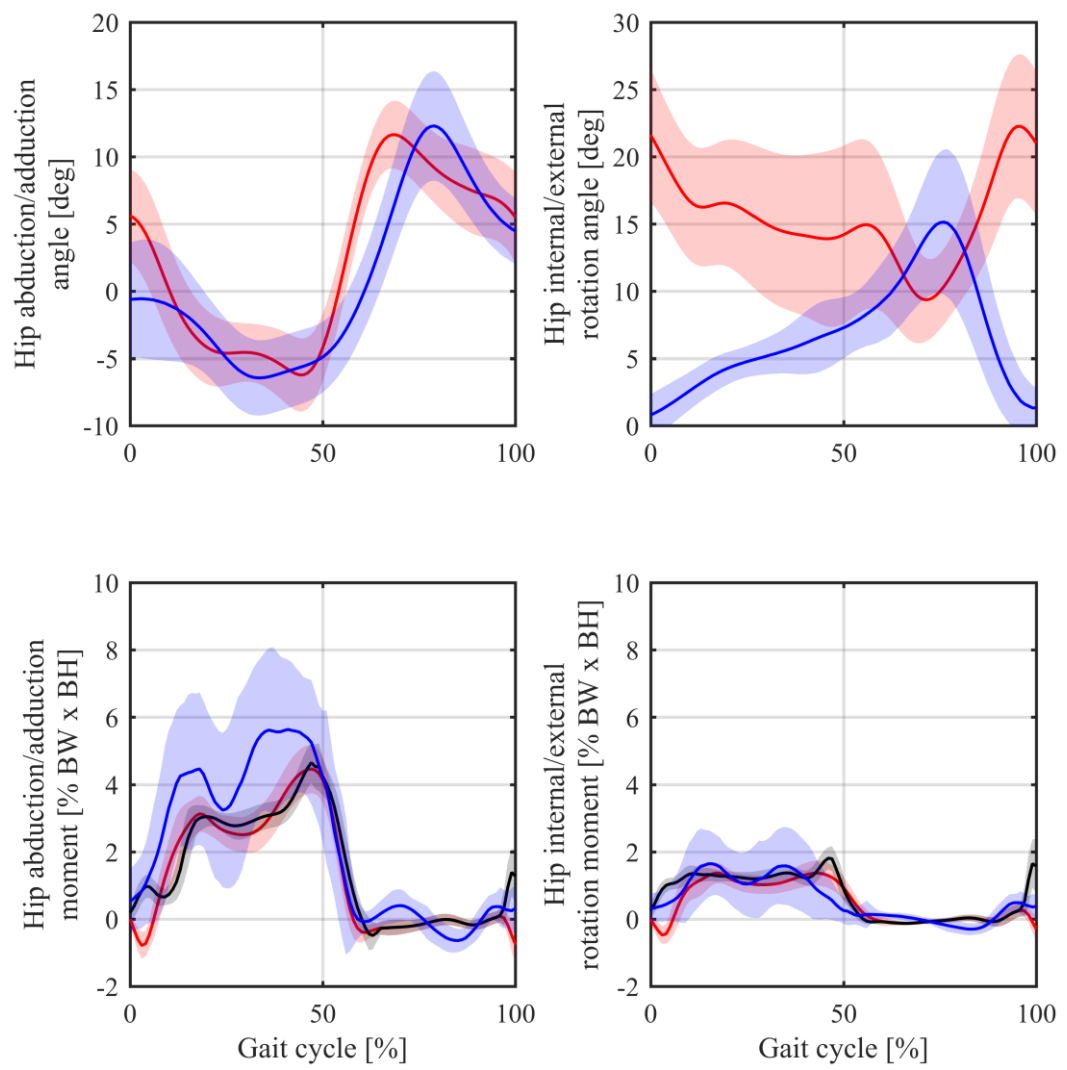


Figure 4

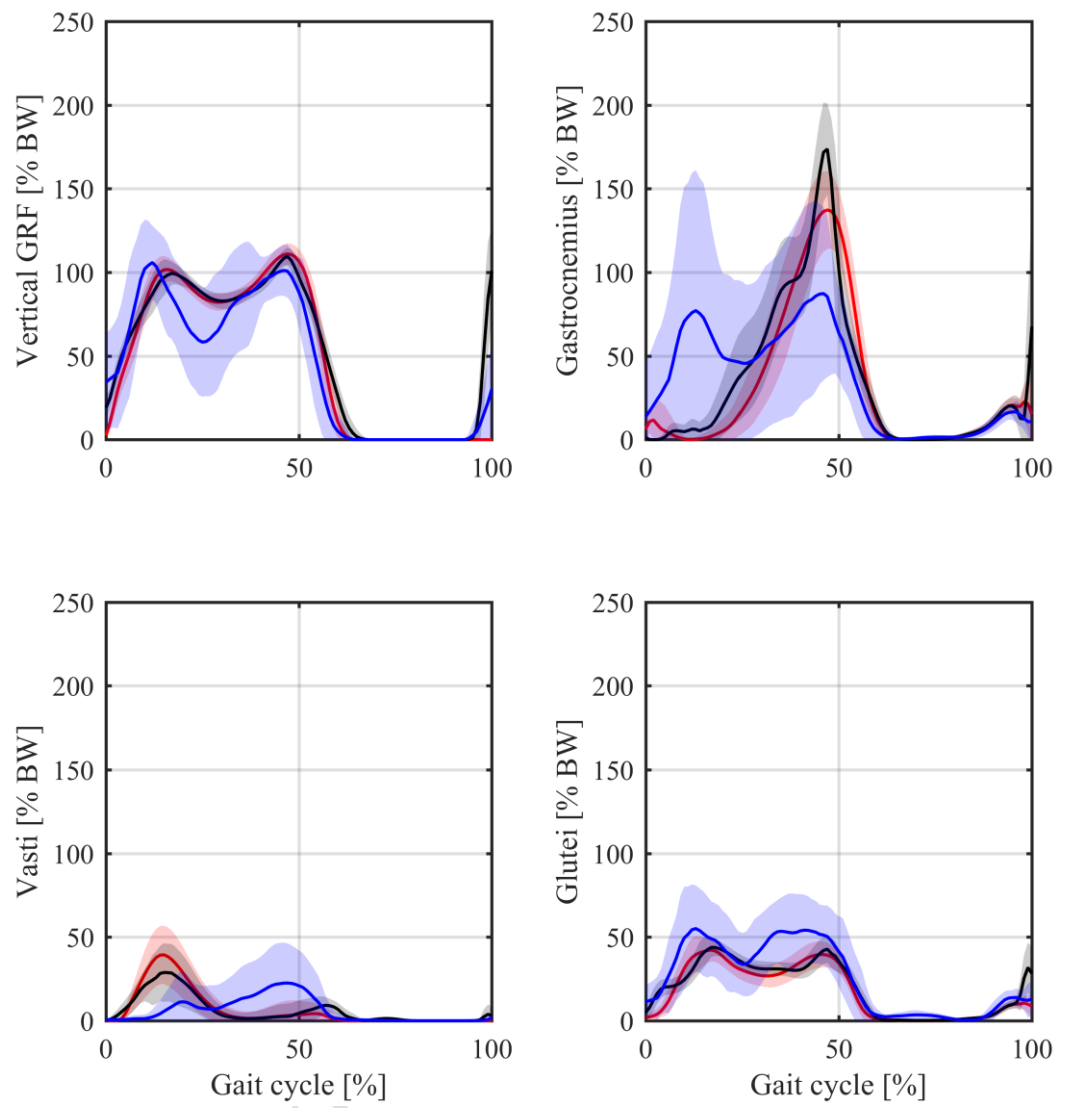


Figure 5

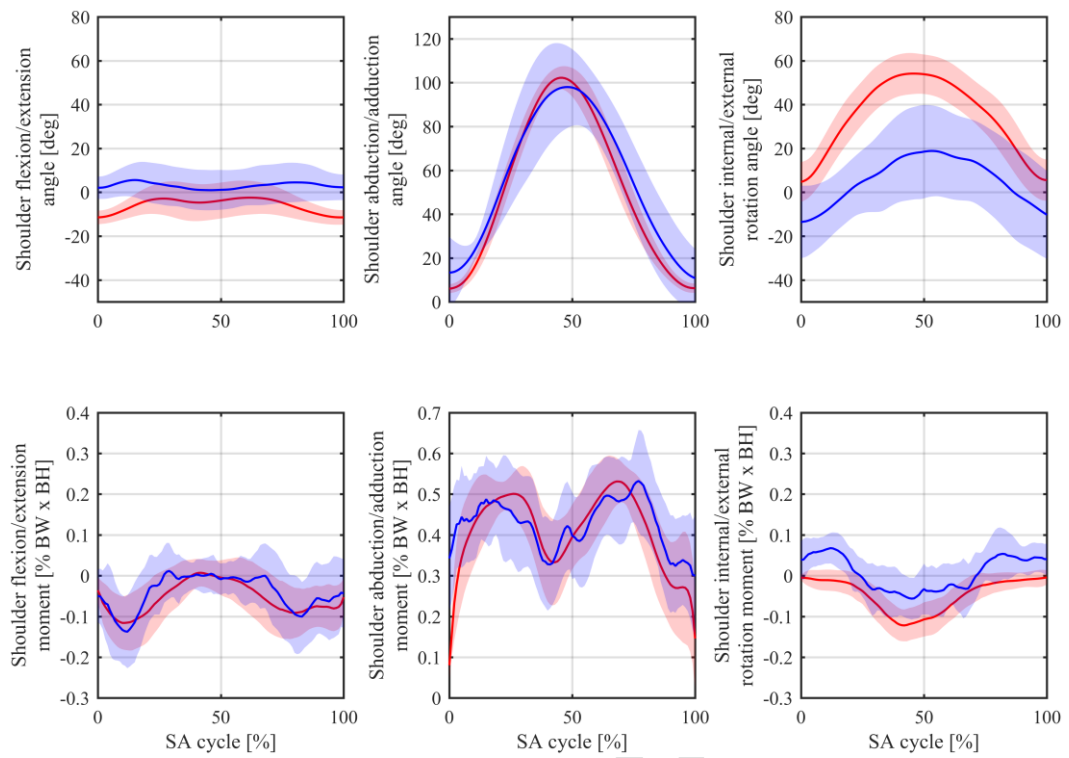


Figure 6

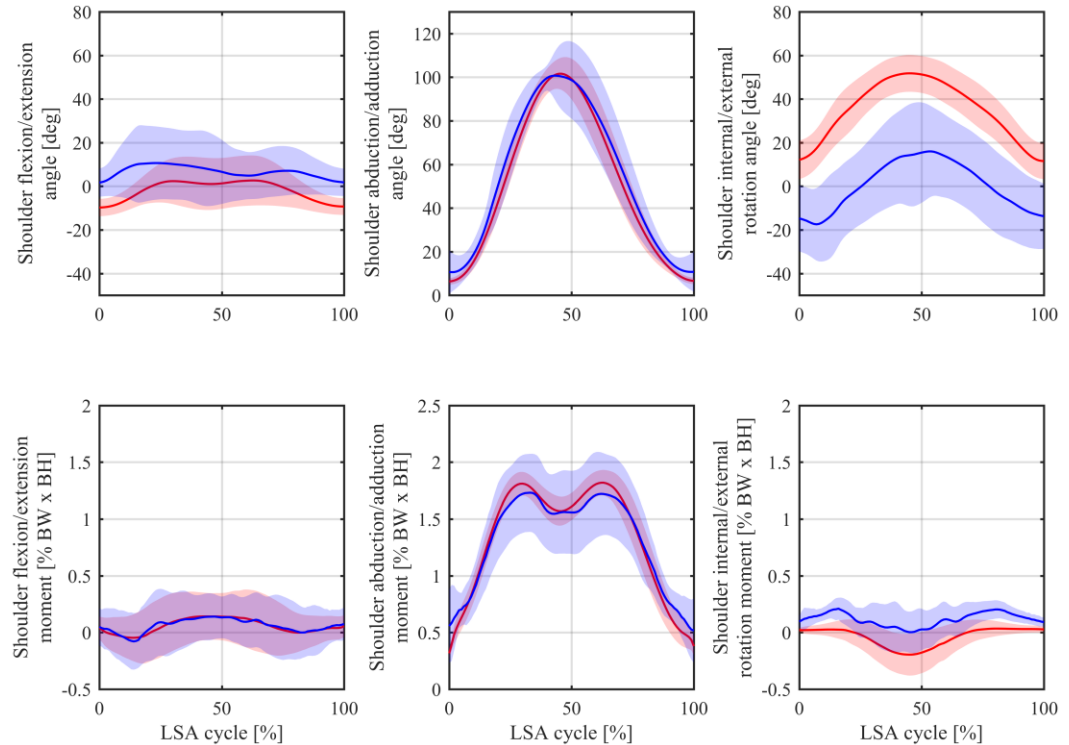
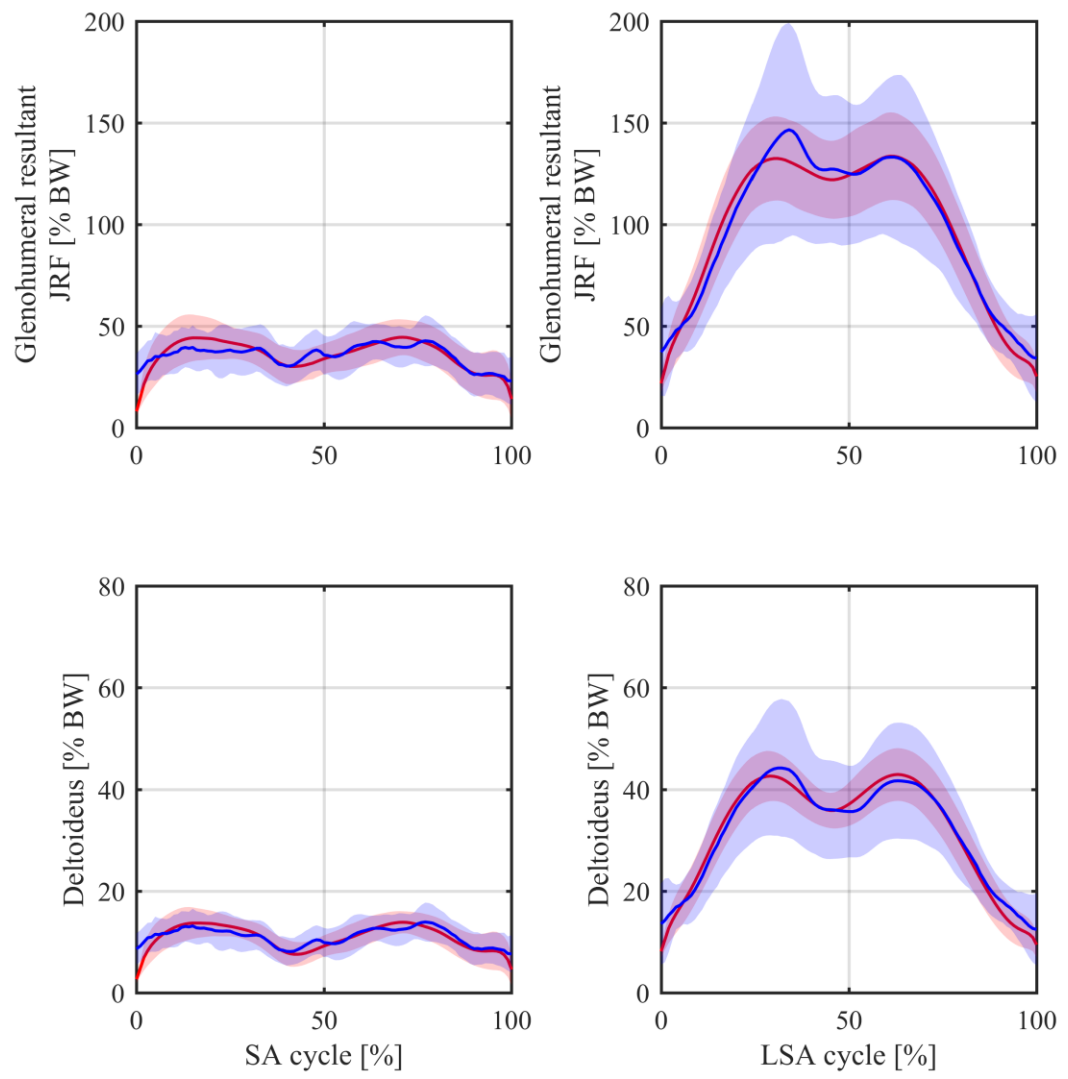
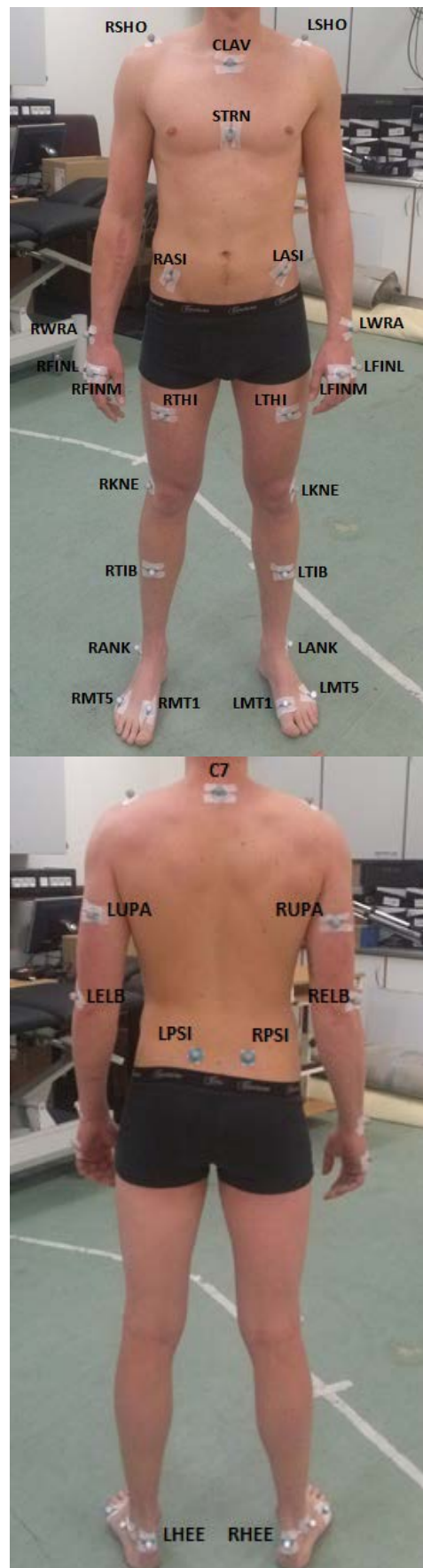


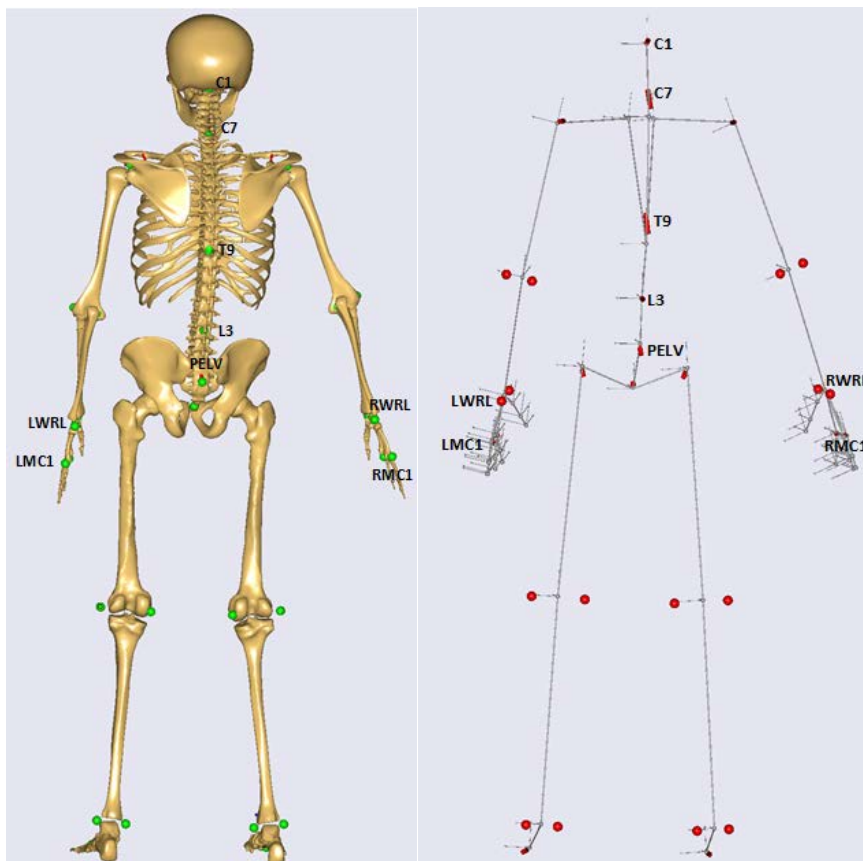
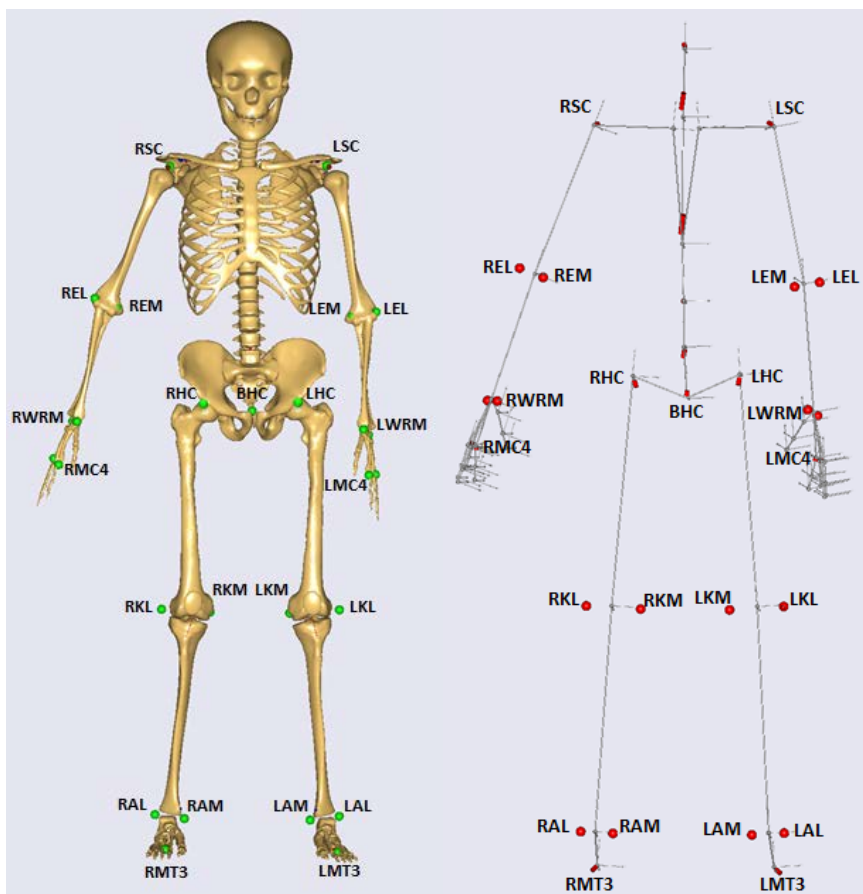
Figure 7



Name	Placement	A/P	M/L	P/D
<i>RTHI</i>	Right thigh	Opt.	Opt.	Opt.
<i>LTHI</i>	Left thigh	Opt.	Opt.	Opt.
<i>RKNE</i>	Right lateral epicondyle	Fix.	Fix.	Fix.
<i>LKNE</i>	Left lateral epicondyle	Fix.	Fix.	Fix.
<i>RPSI</i>	Right posterior superior iliac spine	Opt.	Fix.	Opt.
<i>LPSI</i>	Left posterior superior iliac spine	Opt.	Fix.	Opt.
<i>RASI</i>	Right anterior superior iliac spine	Fix.	Fix.	Fix.
<i>LASI</i>	Left anterior superior iliac spine	Fix.	Fix.	Fix.
<i>RANK</i>	Right lateral malleolus	Fix.	Fix.	Fix.
<i>LANK</i>	Left lateral malleolus	Fix.	Fix.	Fix.
<i>RHEE</i>	Right calcaneus	Fix.	Fix.	Fix.
<i>LHEE</i>	Left calcaneus	Fix.	Fix.	Fix.
<i>RTIB</i>	Right tibia	Opt.	Opt.	Opt.
<i>LTIB</i>	Left tibia	Opt.	Opt.	Opt.
<i>RMT1</i>	Right metatarsus	Fix.	Fix.	Fix.
<i>LMT1</i>	Left metatarsus	Fix.	Fix.	Fix.
<i>RMT5</i>	Right fifth metatarsal	Fix.	Fix.	Fix.
<i>LMT5</i>	Left fifth metatarsal	Fix.	Fix.	Fix.
<i>RELB</i>	Right lateral epicondyle	Fix.	Fix.	Fix.
<i>LELB</i>	Left lateral epicondyle	Fix.	Fix.	Fix.
<i>RWRA</i>	Right wrist bar thumb side	Fix.	Fix.	Fix.
<i>LWRA</i>	Left wrist bar thumb side	Fix.	Fix.	Fix.
<i>RFINL</i>	Right first metacarpal	Fix.	Fix.	Fix.
<i>LFINL</i>	Left first metacarpal	Fix.	Fix.	Fix.
<i>RFINM</i>	Right fifth metacarpal	Fix.	Fix.	Fix.
<i>LFINM</i>	Left fifth metacarpal	Fix.	Fix.	Fix.
<i>RUPA</i>	Right triceps brachii	Opt.	Opt.	Opt.
<i>LUPA</i>	Left triceps brachii	Opt.	Opt.	Opt.
<i>RSHO</i>	Right Acromio-clavicular joint	Fix.	Fix.	Fix.
<i>LSHO</i>	Left Acromio-clavicular joint	Fix.	Fix.	Fix.
<i>STRN</i>	Xiphoid process of the sternum	Opt.	Opt.	Opt.
<i>CLAV</i>	Jugular Notch	Opt.	Opt.	Fix.
<i>C7</i>	7th Cervical Vertebrae	Fix.	Fix.	Fix.



Sup. Figure 1 – Marker-protocol associated to the marker-based system, listing marker name, placement and whether the marker position was fixed (Fix.) or optimized (Opt.) in the anterior/posterior (A/P), medio/lateral (M/L) and proximal/distal (P/D) directions. During the kinematic analysis, the positions of markers placed at identifiable bony landmarks were kept fixed during the optimization procedure, while the positions of markers placed at e.g. the thigh and tibia were optimized. In general, the number of fixed marker positions has to be sufficient to define all model degrees-of-freedom.



Name	Placement
<i>RSC</i>	Right shoulder joint center
<i>LSC</i>	Left shoulder joint center
<i>REL</i>	Right elbow joint lateral
<i>REM</i>	Right elbow joint medial
<i>LEL</i>	Left elbow joint lateral
<i>LEM</i>	Left elbow joint medial
<i>RWRM</i>	Right wrist medial
<i>RMC4</i>	Right fourth metacarpal
<i>LWRM</i>	Left wrist medial
<i>LMC4</i>	Left fourth metacarpal
<i>RHC</i>	Right hip joint center
<i>LHC</i>	Left hip joint center
<i>BHC</i>	Centered between hip joint centers
<i>RKL</i>	Right knee joint lateral
<i>RKM</i>	Right knee joint medial
<i>LKL</i>	Left knee joint lateral
<i>LKM</i>	Left knee joint medial
<i>RAL</i>	Right ankle joint lateral
<i>RAM</i>	Right ankle joint medial
<i>LAL</i>	Left ankle joint lateral
<i>LAM</i>	Left ankle joint medial
<i>RMT3</i>	Right third metatarsal
<i>LMT3</i>	Left third metatarsal
<i>RWRL</i>	Right wrist lateral
<i>RMC1</i>	Right first metacarpal
<i>LWRL</i>	Left wrist lateral
<i>LMC1</i>	Left first metacarpal
<i>C1</i>	First cervical vertebrae
<i>C7</i>	Seventh cervical vertebrae
<i>T9</i>	Ninth thoracic vertebrae
<i>L3</i>	Third lumbar vertebrae
<i>PELV</i>	Center of pelvis

Sup. Figure 2 – Name and placement of virtual markers associated with the marker-less system for the musculoskeletal model (left) and iPi stick figure (right), which enabled the reconstruction of the stick figure movements by the musculoskeletal model. The virtual markers were placed at joint centres and anatomical landmarks that were identifiable on the stick figure.